Protecting the $MoSi_2$ healing particles for thermal barrier coatings using a sol-gel produced Al_2O_3 coating

Carabat, A. L.; Meijerink, M.J.; Brouwer, J. C.; Kelder, E. M.; van Ommen, J. R.; van der Zwaag, S.; Sloof, W. G.

DOI
10.1016/j.jeurceramsoc.2018.02.002

Publication date
2018

Document Version
Final published version

Published in
Journal of the European Ceramic Society

Journal of the European Ceramic Society 38 (2018) 2728–2734

Contents lists available at ScienceDirect

Journal of the European Ceramic Society

journal homepage: www.elsevier.com/locate/jeurceramsoc

Original Article

Protecting the $MoSi_2$ healing particles for thermal barrier coatings using a sol-gel produced Al_2O_3 coating

A.L. Carabat[a,*], M.J. Meijerink[a,b,c], J.C. Brouwer[a], E.M. Kelder[b], J.R. van Ommen[c], S. van der Zwaag[d], W.G. Sloof[a]

[a] Department of Materials Science and Engineering, Delft University of Technology, Mekelweg 2, 2628 CD, Delft, The Netherlands
[b] Faculty of Applied Sciences, Delft University of Technology, Lorentzweg 1, 2628 CJ, Delft, The Netherlands
[c] Department of Chemical Engineering, Delft University of Technology, van der Maasweg 9, 2629 HZ, Delft, The Netherlands
[d] Faculty of Aerospace Engineering, Delft University of Technology, Kluyverweg 1, 2629 HS, Delft, The Netherlands

ARTICLE INFO

Keywords:
Self-healing thermal barrier coatings
$MoSi_2$
Alumina shell
Sol-gel

ABSTRACT

A successful sol-gel process to encapsulate molybdenum di-silicide $MoSi_2$ particles with a closed and thermally stable Al_2O_3 layer using aluminium tri-sec-butoxide as a precursor is presented. The processing conditions such as precursor selection and temperature were optimized through analysing the interaction of the $MoSi_2$ particles with the sol. The application of the sol-gel based coating was followed by calcining the coated particles at temperatures between 900 and 1200 °C in Ar. The shell composition and the mechanical stability of the microcapsule were analysed by means of X-ray diffraction, scanning electron microscopy and thermogravimetric analysis. Upon calcining at 1200 °C in Ar, the $MoSi_2$ core remains intact as it is, covered by an α - alumina shell with a thickness of about 0.6 μm. The stability tests proved that the encapsulate particles are about five times more oxidation resistant than the uncoated $MoSi_2$ particles.

1. Introduction

Molybdenum di-silicide not only is an attractive monolithic high temperature material because of its excellent refractory and mechanical properties [1–6], but is also as attractive candidate for repairing crack damage in brittle ceramic coatings such as in thermal barrier coatings (TBCs) [7,8]. TBCs are often applied to metallic surfaces of combustion chambers, blades and vanes in gas turbines and jet engines to protect them from corrosion and oxidation at elevated temperatures [9,10]. Yttria stabilized zirconia (YSZ, ZrO_2 containing 4–5 mol% Y_2O_3) is the most employed TBC material due to its excellent chemical and thermo-mechanical properties, such as low thermal conductivity at elevated temperatures (2.3 $W\,m^{-1}\,K^{-1}$), low density (6.4 g/cm^3), high melting point (2700 °C), high toughness (7.7 $MPa\,m^{0.5}$) and good corrosion resistance [9–11]. However, the durability of the TBCs is negatively affected by thermal cycling due to the starts and the stops of the engine resulting in temperatures varying over more than 1000 °C. High compressive stresses develop in the coating during cooling as a result of the mismatch between the coefficients of thermal expansion of the metal substrate ($14{\cdot}10^{-6}\,°C^{-1}$) and that of the YSZ TBC ($10–11{\cdot}10^{-6}\,°C^{-1}$) [11,12]. As a consequence, microcracks form within the ceramic coating. They propagate and coalesce during subsequent thermal cycling leading to coating debonding and ultimately engine failure [11,13–15].

As YSZ TBCs are thermodynamically stable and hence do not poses autonomous crack-healing capabilities, a self-repair mechanism active at the high temperature encountered in a turbine engine is highly desirable to prolong the lifetime of these coatings. The concept of autonomous high temperature crack-healing based on the presence of $MoSi_2$ sacrificial particles embedded in a YSZ matrix has been presented elsewhere [7,16]. It is based on the release of viscous silica (SiO_2), that fills the crack running through the matrix and re-establish the adherence in the ceramic coating. Subsequently, the formed SiO_2 reacts with the matrix via a solid-state reaction, resulting in a load bearing crystalline zircon phase ($ZrSiO_4$), which gives a better adhesion between the healing agent and the fractured surface. However, in porous yttria partially stabilized zirconia based TBC matrix the transport of oxygen ions is likely to prevail [17]. This will lead to the premature oxidation of $MoSi_2$ particles and, consequently, offsetting the healing reaction even in the absence of a crack. Thus, the presence of an inert and oxygen impenetrable shell around the actual intermetallic particles is critical to prevent the premature triggering of the healing mechanism and to keep the particles in a dormant state. α-Alumina seems an ideal candidate to protect the $MoSi_2$ particles from premature oxidation since

* Corresponding author.
E-mail address: a.l.carabat@tudelft.nl (A.L. Carabat).

https://doi.org/10.1016/j.jeurceramsoc.2018.02.002
Received 25 August 2017; Received in revised form 24 January 2018; Accepted 1 February 2018
Available online 08 February 2018

it has a good thermal stability [18] and a low permeability for oxygen [19,20]. Hence, the healing mechanism will become active only when a crack penetrates the alumina shell protecting the active $MoSi_2$.

Several soft-chemical routes have been proposed to deposit alumina shell such as: precipitation [21,22], hybridization [23] and sol-gel [24]. Among them, the sol-gel method is the most economical way to develop coatings of sizeable thickness and to generate solids of high purity [25]. So far, alumina coatings have been applied successfully on silicon containing particles such as silicon carbide (SiC) grit and $MoSi_2$ to improve their oxidation and corrosion resistance [21,26,27]. However, in the case of $MoSi_2$-Al_2O_3 core-shell system in which the protective α alumina layer was produced by a precipitation reaction, a rather thin layer of alumina – silica mixed oxides of only 0.15 μm was obtained after annealing at 1000 °C [21].

The current paper aims to create a closed and continuous thicker shell of α alumina around $MoSi_2$ intermetallic particles through a simple sol-gel approach. Experimental results proved that by tuning the processing conditions (i.e. type of precursor and calcining temperature), a robust and stable shell of α alumina with a typical thickness of 0.6 μm could be obtained.

2. Experimental details

2.1. Materials

The chemicals for the sol-gel coating of $MoSi_2$ particles were aluminium oxalate tetrahydrate ($Al_2(C_2O_4)_3 \cdot 4H_2O$, 99% purity, Alfa Aesar, Karlsruhe, Germany), aluminium tri-isopropoxide ($Al(OC_3H_7)_3$, 98% purity, Sigma-Aldrich Co., St. Louis, Missouri, US), aluminium-tri-sec-butoxide ($Al(OC_4H_9)_3$, 97% purity, Sigma Aldrich Co., St. Louis, Missouri, US), nitric acid (HNO_3 99% purity, 65 wt% solution as a source, Sigma-Aldrich Co. St. Louis, Missouri, US), isopropanol (C_3H_8O, 99.8%, Sigma-Aldrich Co., St. Louis, Missouri, US), ethanol (C_2H_6O, 99.8%, Sigma-Aldrich Co., St. Louis, Missouri, US), molybdenum disilicide ($MoSi_2$, 99.5% purity, particle size of 29 μm; ChemPur GmbH, Karlsruhe, Germany) and deionized water (18.2 MΩ cm at 25 °C). All chemicals were used without any further purification.

2.2. $MoSi_2$-Al_2O_3 core-shell synthesis

To produce sol-gel encapsulated $MoSi_2$ particles, a modified Yoldas method [28,29] was employed. This method is based on a polycondensation reaction leading to the formation of a boehmite sol, which upon further annealing transforms into a dense and defect free α-alumina layer.

Prior to the encapsulation process, the $MoSi_2$ powder was wind sifted to remove the fine fraction and the impurities. Wind sifting was performed using an Alpine 100 MRZ laboratory zig-zag classifier (Alpine Multi-Plex 100 MRZ, Hosokawa Micron Powder System, Summit, New Jersey, USA). Airflow was fixed at 15 m^3/h and the classifier rotational speed was kept at 5000 rpm. The wind sifting resulted in a powder having an average particle diameter of 30 μm with a D_{10} and D_{90} value of 10 and 60 μm, respectively, as will be described further on.

Three precursors were selected and tested to obtain more detailed information on the reaction of $MoSi_2$ particles with the sol: aluminium oxalate ($Al_2(C_2O_4)_3$), aluminium tri-isopropoxide ($Al(OC_3H_7)_3$) and aluminium tri-sec-butoxide ($Al(OC_4H_9)_3$), respectively. The experiments were performed in a reactor consisting of a glass beaker (1000 mL) positioned on a magnetic stirring hot plate (IKA RET control-visc, IKA – Werke GmbH & Co, Staufen, Germany) with thermocouple to control the temperature of the sol and a magnetic stir bar with controlled speed. Nitrogen gas (5 N purity) was supplied to the reactor by a custom-made ring-shaped bubbler with a flow rate of 200 sccm, to ensure a better dispersion of the healing particles in the sol suspension by reducing the rate of oxidation.

First, aluminium oxalate tetrahydrated was dissolved in 20 mL of 1.0 M HNO_3 solution and 20 mL deionized water (Mili-Q ultrapure water type 1; 18.2 MΩ cm at 25 °C), to obtain a molar ratio of 1:110 of $Al_2(C_2O_4)_3 \cdot 4H_2O$ to H_2O. Then, the suspension was heated to 60 °C and stirred for 30 min at 800 rpm to dissolve the aluminium oxalate. Next, $MoSi_2$ particles (10 g) with an average size of 30 μm were added to the solution and the temperature was increased to 80 °C to initiate the gelation of the aluminium oxalate around the particles. The as-formed mixture was kept at this temperature for 90 min while continuing stirring.

In the case of aluminium tri-isopropoxide, the precursor was dissolved in 200 mL isopropanol and 50 mL ethanol with a molar ratio of 1–70 of $Al(OC_3H_7)_3$ to C_3H_8O. 10g of $MoSi_2$ powder was dispersed in 72 mL deionized water and 72 mL of isopropanol by ultrasonication, prior to the sol-gel process. After, the dispersed powder was added to the dissolved $Al(OC_3H_7)_3$ solution, together with 3mL of 1.0 M HNO_3 solution. The mixture was heated to 90 °C and left to gelate for 30 min.

The sample based on aluminium tri-sec-butoxide was prepared by heating a mixture of 600 mL of deionized water and 15 ml of 1.0 M HNO_3 to 80 °C to obtain a molar ratio of 1 : 150 of $Al(OC_4H_9)_3$ to H_2O. First, 10 g of $MoSi_2$ powder was added in the solution mixture of deionized water and HNO_3 and 200 sccm nitrogen (5N purity) was purged through the suspension to improve the dispensability of the particles in the solution. When the temperature was stable at 80 °C again, 10 g of $Al(OC_4H_9)_3$ was added with approx. 25 mL of ethanol to transfer the viscous liquid. After, the system was left to gelate for 60 min. Next, the nitrogen flow and stirring were stopped and the solution was left at 80 °C until the liquid fraction was evaporated.

All the three resulting gels were filtered using a glass - vacuum filtration system (Sartorius Stedium, Biotech, Goettingen, Germany) with a hydrophilic propylene membrane with a pore size of 0.45 μm. To remove the unreacted precursors, the samples were washed with warm deionized water (about 60 °C). Finally, the coated particles were dried in an autoclave (WTC binder, TAMSON, Tuttlingen, Germany) at 110 °C overnight and gently ground to break up the agglomerates.

To improve the structural integrity of the coating and obtain a thicker shell, the molar ratio of the selected precursor (aluminium tri-sec-butoxide) was increased from 1:150 to 2:150 of $Al(OC_4H_9)_3$ to H_2O, following the same coating procedure, as described above; see Fig. 1. Next, the coated particles were subjected to a two-step annealing treatment. First, a calcination treatment was applied at 450 °C for 30 min in laboratory air and 15 h in Ar, to slowly release the molecular water, followed by a post-treatment between 900 and 1200 °C for 1 h in Ar, to consolidate and to promote the formation of α-Al_2O_3 shell.

2.3. Characterisation

The particles size distribution of the wind sifted $MoSi_2$ particles was determined with a laser diffraction instrument (Malvern Mastersizer X, Malvern Instruments Ltd, Worcestershire, UK). Prior to the measurement, the particles were dispersed in water for 20 min by applying ultrasonic vibration.

The morphology of the sol-gel $MoSi_2$ coated particles was investigated by scanning electron microscopy (SEM) using a JSM 6500F (JEOL, Tokyo, Japan) operated with an electron beam energy of 15 keV and a beam current of approx. 600 pA. Prior to the SEM observation, the particles were coated with a thin carbon film to prevent charging.

The shell and core composition was analysed with X-ray diffractometry (XRD). A Bruker D500 diffractometer equipped with a Huber incident-beam monochromator and a Braun PSD detector operated with Cu Kα1 (1.54060 pm wavelength) was used to record the diffractograms in the 2θ range of 15–70° with a step size of 0.0387° 2θ.

The shell integrity was investigated by exposure of the coated particles to a quasi-stagnant oxidizing environment at high temperatures using a thermogravimetric analysis (TGA). For this purpose, a symmetrical thermogravimetric analyser (Setaram TAG 16/18, France) was

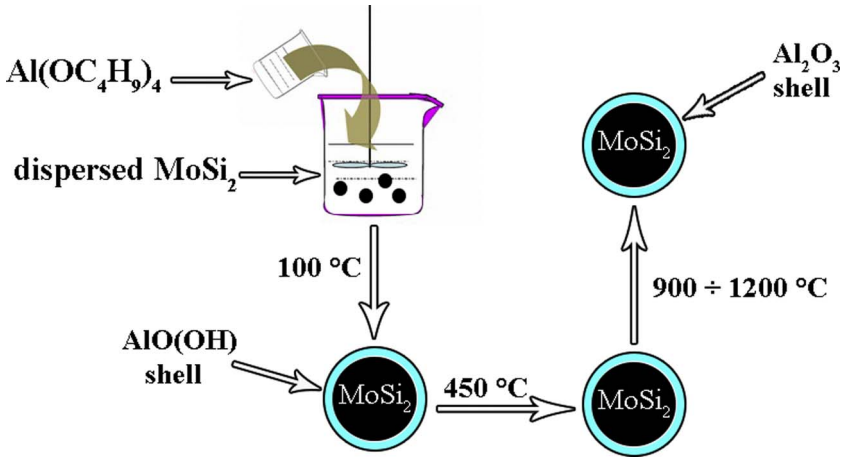

Fig. 1. Schematic of sol-gel coating of $MoSi_2$ healing particles using aluminium tri-sec butoxide as a precursor. The set up consist of a glass beaker fixed on a heating and stirring plate. Nitrogen was supplied to the reactor by a custom made ring-shaped bubbler to ensure a good dispersion of the $MoSi_2$ healing particles.

used. First, the decomposition kinetics of the uncoated $MoSi_2$ particles was investigated by monitoring the weight change during isothermal hold at 1100 °C for 100 h in synthetic air (20 vol.% oxygen in nitrogen). Thereafter, the core-shell system was analysed under the same conditions. The typical mass of each 'sample' was about 200 mg which corresponds to about $2.12 \cdot 10^7$ particles.

3. Results and discussion

3.1. Oxidation kinetics of the uncoated $MoSi_2$ particles

The thermal response of the uncoated $MoSi_2$ particles was recorded by monitoring the weight change with the temperature using a symmetrical thermogravimetric analyser; see Fig. 2. Since oxygen was readily available to react with the unprotected $MoSi_2$ core particles, a rapid weight gain was recorded between 450 and 600 °C. This is associated with the concomitant formation of MoO_3 whiskers and SiO_2 clusters [30]. Above 600 °C, the mass gain becomes almost constant due to the formation of a passive layer of SiO_2 around the $MoSi_2$ particles. However, as temperature increases (> 800 °C), gaseous MoO_3 forms due to the cracking of the passive SiO_2 layer [31], resulting in a weight loss; see Fig. 2.

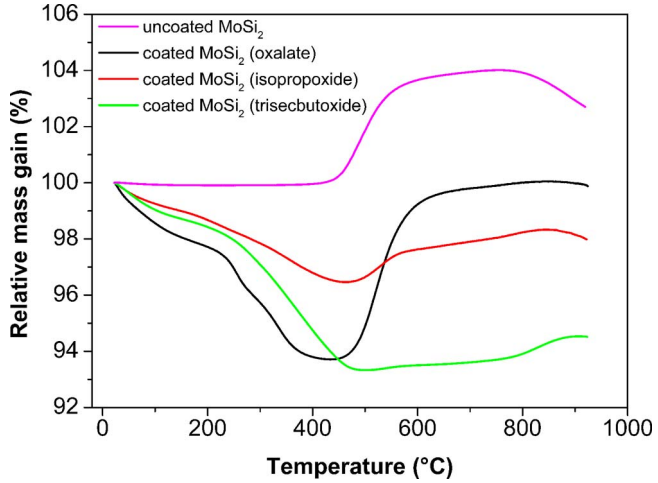

Fig. 2. Mass gain versus temperature during exposure in synthetic air (20 vol. % O_2 in N_2) with heating rate 5 °C/min of uncoated and coated $MoSi_2$ particles with a sol derived from aluminium oxalate, aluminium iso - propoxide and aluminium tri-sec-butoxide precursors.

3.2. Oxidation kinetics of $MoSi_2$ particles coated with the 'green' sol-gel coating

The mass change of the three samples consisting of 'green' (i.e. uncalcined) coated particles versus the temperature is shown in Fig. 2. A large mass decrease was recorded between 100 and 500 °C for the all three type of precursors. Three reaction regimes can be distinguished: (i) from room temperature to 150 °C, the evaporation of physical bonded water and residual solvent occurs; (ii) the temperature region of 150 to approx. 350 °C, is assigned to the desorption of chemically bonded water and the decomposition of the unreacted precursor in the gel, and (iii) from 350 to about 500 °C, the dehydroxylation reaction of boehmite to γ-Al_2O_3 takes place [32,33]. A major weight gain was observed between 600 and 900 °C for the $MoSi_2$ particles coated by the sol with either aluminium oxalate or aluminium isopropoxide, indicating a poor coverage of the healing particles, thus leading to the oxidation of the core. Furthermore as shown in Fig. 2 the precursor was not fully converted into boehmite and alumina. In the case of the sol derived from aluminium tri-sec-butoxide a smaller weight gain was recorded and the weight became constant at 800 °C (see Fig. 2), indicating that the precursor fully coated the healing particles and was converted into boehmite. Hence, aluminium tri-sec-butoxide was selected as an optimum precursor for the further sol-gel encapsulation process.

3.3. Shell morphology and composition after deposition and drying

A comparison of the morphology of uncoated and coated $MoSi_2$ particles using aluminium tri-sec-butoxide as a precursor is presented in Fig. 3. The recorded images revealed that the surface of the coated $MoSi_2$ particles is completely covered by a closed layer; see Fig. 3b.

The X-ray diffractogram of the coated particles revealed both peaks belonging to $MoSi_2$ and smaller peaks corresponding to boehmite in a pseudo-crystalline state [34]; see Fig. 4.

3.4. Shell composition after calcining

The integrity of the shell should be maintained during the phase transformation of boehmite to α – Al_2O_3 through the calcining process. When annealing, the boehmite shell undergoes several phase transformations which are associated with volume change [35–37]. The most critical volume change ($\Delta V/V = -29.4\%$) occurs between 300 and 500 °C, when the dehydroxilation of AlO(OH) takes place [21]. Thus, to avoid the fragmentation of the boehmite shell, the encapsulated particles were first exposed at 450 °C to gradually release the molecular water, followed by a gradual increase of the calcining temperature from

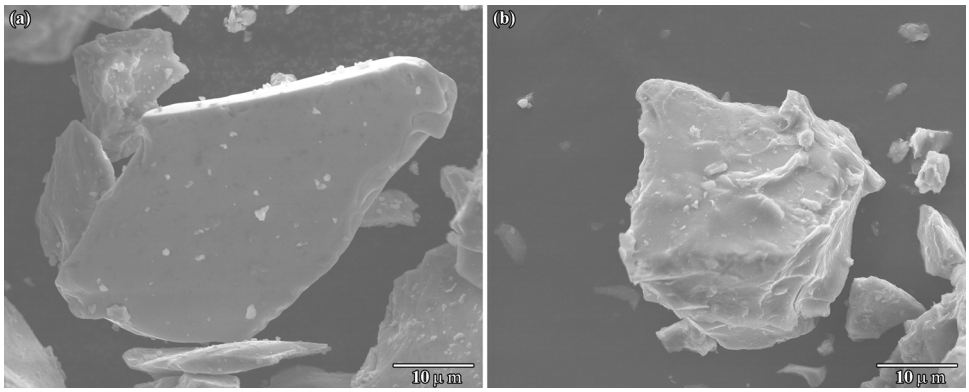

Fig. 3. Surface morphology of uncoated and sol-gel coated $MoSi_2$ particle after drying at 80 °C overnight: (a) as received and (b) boehmite-coated particles by using aluminium tri-sec-butoxide as a precursor.

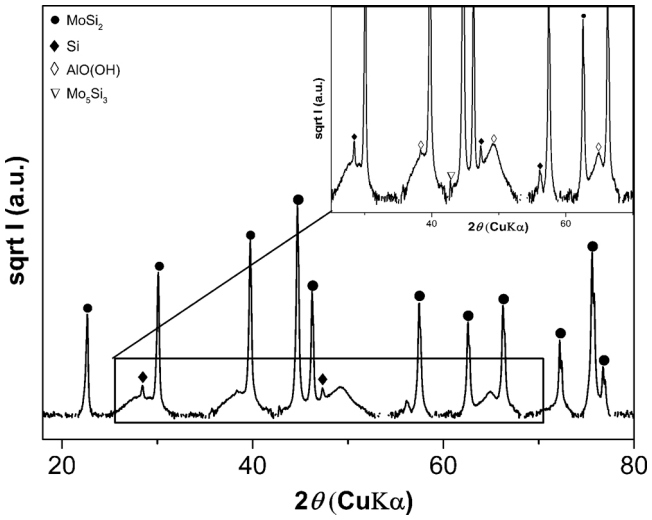

Fig. 4. X-ray diffraction pattern of sol-gel coated $MoSi_2$ particles using aluminium tri-sec-butoxide precursor after drying in air at 80 °C overnight. Peaks between 30 and 70° 2θ, display the formation of AlO(OH).

900 to 1200 °C, to identify the phase transformation after each annealing step; see Fig. 5. The XRD analysis reveal that the $MoSi_2$ core remained intact at all the annealing temperatures. Only after annealing at 1200 °C, the diffraction lines corresponding to θ, δ and α-Al_2O_3 were observed in addition to those for the $MoSi_2$ tetragonal phase; see enlargement Fig. 5.

3.5. Alumina shell thickness

The alumina shell thickness was measured from SEM images of cross-sections of the encapsulated $MoSi_2$ core-shell particle after calcining at 1200 °C. A representative cross section is shown in Fig. 6. The shell is continuous, however, not of a constant thickness as the healing particles are of irregular shape. The layer was thinnest at the sharp edges of $MoSi_2$ particles [27]. The average layer thickness of the coated $MoSi_2$ particle was determined to be about 0.6 μm; see Fig. 6.

3.6. Microcapsule stability

The stability of the encapsulated particles at high temperature was investigated via thermogravimetric analysis; see Fig. 7. The weight gain of the uncoated and coated $MoSi_2$ particles calcined at 1200 °C was measured after exposure to 1100 °C in synthetic air for 100 h. The uncoated particles increase in weight due to the oxidation of $MoSi_2$ core. For the encapsulated particles, a smaller mass increase in the initial slope is observed. This can be associated with the partial oxidation of the $MoSi_2$ core via cracks that may form in the alumina shell, during the stability test. About five times lower weight gain was observed for the alumina encapsulated $MoSi_2$ particles as compared to the uncoated $MoSi_2$; see Fig. 7. This indicates that during the stability test, the encapsulated particles are more stable than the $MoSi_2$ in as received conditions and the alumina shell acts as a protective layer against severe oxidation. The oxygen partial pressure at the interface between the $MoSi_2$ particle and the alumina shell is governed by the dissociation partial pressure of Al_2O_3 (i.e. about 10^{-33} atm at 1100 °C), which is too low to form SiO_2 (which requires about 10^{-24} atm at 1100 °C). However, when defects like pores or cracks are present in the alumina shell, the $MoSi_2$ may be exposed to higher oxygen partial pressures causing silica to form.

The microstructure of the uncoated and coated particles calcined at 1200 °C and subsequently exposed at 1100 °C in air for 100 h is shown in Fig. 8. In the absence of the alumina shell, all the unencapsulated particles oxidized and, as a result, a uniform and amorphous SiO_2 layer developed on their surface; see Fig. 8a and b. In contrast, the encapsulated $MoSi_2$ particles remained intact after isothermal exposure at 1100 °C; see Fig. 8c. However, a few of the alumina coated particles displayed fine cracks at the surface; see Fig. 8d. This may be caused by the presence of θ-Al_2O_3 phase in the shell which has not been fully converted to α-Al_2O_3 after 1 h of calcining at 1200 °C; see enlargement in Fig. 5. During the thermal stability test, the phase transformation of θ-Al_2O_3 to α-Al_2O_3 occurs along with a volume change of about −10% [21]. This volume shrinkage generates a large strain misfit, which cannot be accommodated by the plastic deformation of the crystalline α-Al_2O_3, thus leading to the crack formation in the shell.

Due to alumina shell cracking, the $MoSi_2$ core is exposed to the oxidizing environment and a thin layer of SiO_2 forms during the thermal stability test. Assuming that the total volume of the particle after the test comprises the volume of the $MoSi_2$ core and the volume of the silica shell (see Fig. 9), then the thickness of the SiO_2 layer formed during the 100 h of exposure can be estimated using the following relation:

$$V_{total} = V_{particle} + V_{shell} \tag{1}$$

If the $MoSi_2$ particle has a spherical shape and a diameter d, then Eq. (1) can be rewritten as:

$$\frac{1}{6}\pi\cdot\left(d_{particle} + \delta_{SiO_2}\right)^3 = \frac{1}{6}\pi\cdot d^3 + \frac{m_{SiO_2}}{\rho_{SiO_2}} \tag{2}$$

where

$$m_{SiO_2} = n_{SiO_2}\cdot M_{SiO_2} \tag{3}$$

with n_{SiO_2} moles of SiO_2 and M_{SiO_2} the molar mass of silica.

If all the Si is depleted, then $n_{SiO_2} = n_{Si}$ and thus Eq. (3) becomes:

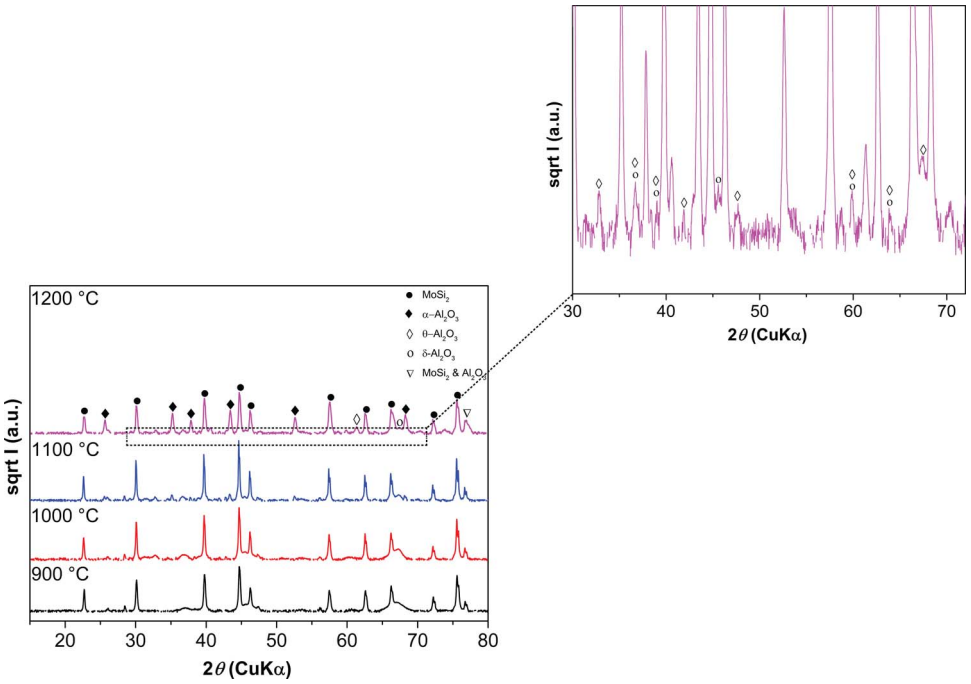

Fig. 5. X-ray diffraction pattern of encapsulated $MoSi_2$ particles pre-calcined at 450 °C for 12 h in Ar followed by calcination at different temperatures: (a) 900 °C, (b) 1000 °C, (c) 1100 °C and (d) 1200 °C for 1 h in Ar. The enlargement between 30 and 70° 2θ displays the formation of metastable alumina phases (θ- and δ-Al_2O_3).

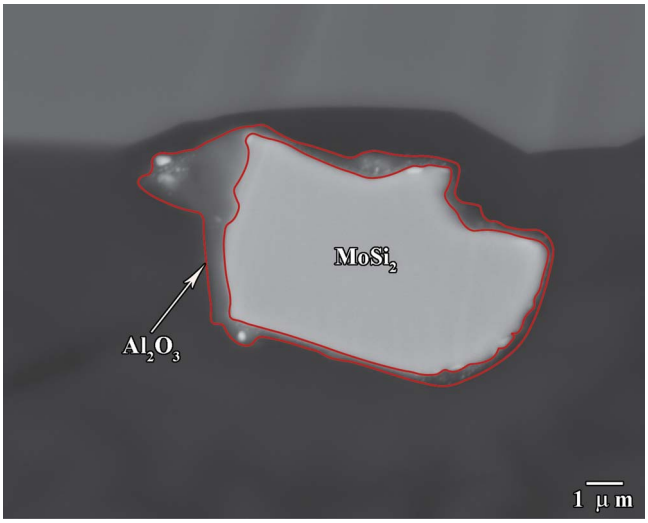

Fig. 6. Cross-section image of encapsulated $MoSi_2$ particle with a shell of Al_2O_3 after annealing at 1200 °C for 1 h in Ar.

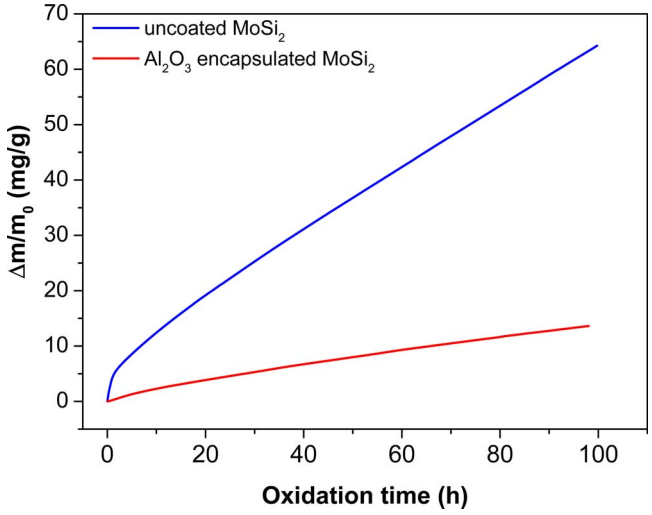

Fig. 7. Mass gain versus isothermal exposure at 1100 °C in synthetic air (20 vol.% O_2 in N_2), for 100 h of: (a) uncoated and (b) coated $MoSi_2$ – Al_2O_3 core-shell particles calcined at 1200 °C.

$$m_{SiO_2} = n_{Si} \cdot M_{SiO_2} \tag{4}$$

with $n_{Si} = m_{Si}/M_{Si}$ and m_{Si} equals the wt % of Si in $MoSi_2$, then Eq. (4) can be rewritten as:

$$m_{SiO_2} = x \cdot wt\%Si \cdot m_{particle} \frac{M_{SiO_2}}{M_{Si}} \tag{5}$$

And

$$m_{particle} = V_{particle} \cdot \rho_{particle} \tag{6}$$

Then, Eq. (2) can be re-arranged in terms of Eqs. (5) and (6):

$$\delta = d\left[\left(1 + x \cdot wt\%Si \cdot \frac{M_{SiO_2} \cdot \rho_{particle}}{\rho_{SiO_2} \cdot M_{Si}}\right)^{1/3} - 1\right] \tag{7}$$

However, Eq. (7) holds for case when all the $MoSi_2$ is fully transformed into SiO_2. Knowing the mass gain of the uncoated and encapsulated particles after isothermal exposure at 1100 °C (see Fig. 7), Eq. (7) can be re-written as:

$$\delta = d \cdot \left[\left(1 + x \cdot \frac{\Delta m_{MoSi_2} \cdot \rho_{MoSi_2}}{m_{MoSi_2} \cdot \rho_{SiO_2}}\right)^{1/3} - 1\right] \tag{8}$$

where x is the amount of Si in $MoSi_2$ (30 wt %), ρ_{SiO_2} and ρ_{MoSi_2}– are the density of SiO_2 and $MoSi_2$ particles, respectively, while Δm_{MoSi_2} and m_{MoSi_2} are the mass gained after the stability test corresponding to the oxidation of $MoSi_2$ particles to SiO_2 and the initial mass of $MoSi_2$ particles before the stability test. For the encapsulated $MoSi_2$ particles studied here it is estimated that a layer of SiO_2 with a thickness of about 90 nm is formed during the stability test at 1100 °C as a result of partial exposure of the healing particle via the micro-cracks in the alumina shell. Applying the same relation for the uncoated $MoSi_2$ particles (Eq.

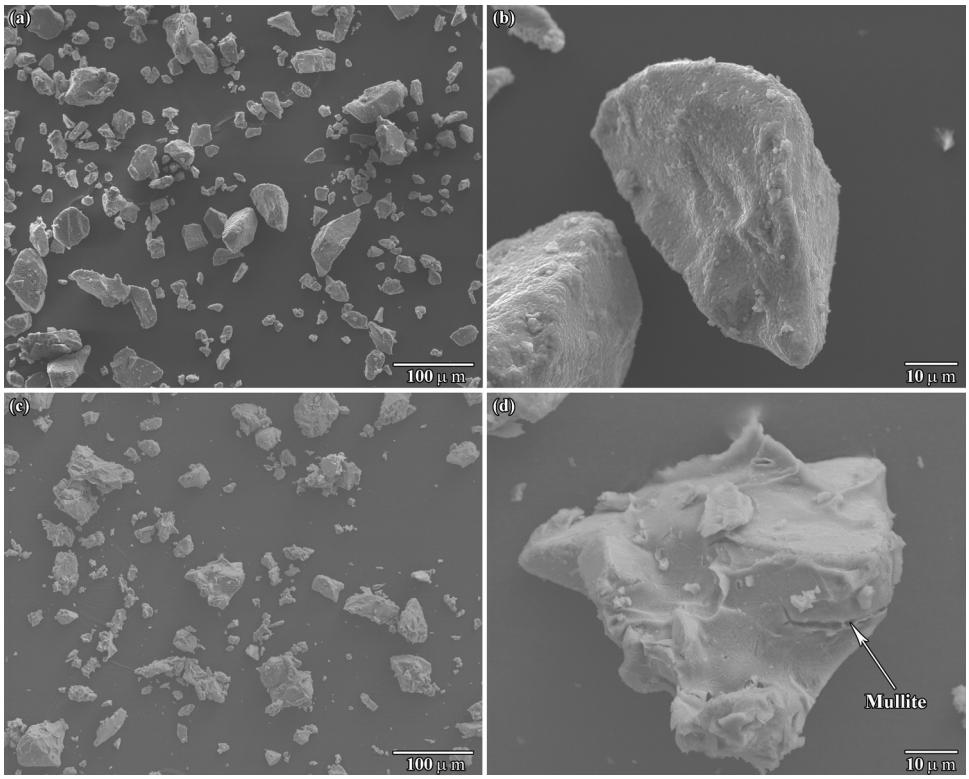

Fig. 8. Shell morphology of uncoated (a), (b) and alumina encapsulated $MoSi_2$ particles calcined at 1200 °C (c) and (d), after oxidation test at 1100 °C for 100 h in synthetic air (20 vol.% O_2 in N_2).

(8)), a SiO_2 layer with a thickness of about 400 nm is estimated to form during the isothermal exposure.

In addition, the resulting SiO_2 inside the crack either reacts with the existing alumina shell to form mullite [38] (see Fig. 8d) or transforms to cristobalite. This is supported by the XRD analysis, where Mo_5Si_3, cristobalite (as a result of $MoSi_2$ oxidation) and mullite were observed in addition to $MoSi_2$ and α-Al_2O_3 peaks; see Fig. 10. However, the intensity of cristobalite and mullite peaks are very low, confirming that most of the alumina encapsulated particles preserved their integrity during isothermal exposure at 1100 °C. In addition, the mass change of these encapsulated particles becomes almost monotonic during the remainder of the stability test as a result of mullite formation inside the crack; see Fig. 7. Also mullite preserves the $MoSi_2$ core, since its diffusivity at 1100 °C is comparable with that of alumina ($1.2{\cdot}10^{-20}$ [39] versus $4.6{\cdot}10^{-18}$ m^2/s [40]).

4. Conclusions

Coarse and irregular $MoSi_2$ healing particles of about 30 μm were successfully encapsulated via sol-gel method. Lower calcining temperatures (i.e. 900 ÷ 1100 °C) promoted the formation of a metastable δ-Al_2O_3 phases. Only after calcining at 1200 °C in Ar, a closed α alumina shell of about 0.6 μm thickness was formed. The oxidation test confirmed that the particles remained intact after 100 h exposure in air at 1100 °C as they had a five times lower mass gain than the uncoated $MoSi_2$ particles. The shell morphology after the oxidation test indicated that the healing particles partially reacted with alumina shell to form mullite, providing further protection against oxidation.

Acknowledgements

This project has received funding from European Union Seventh Framework Programme (FP7/2007-2013) under grant agreement n°

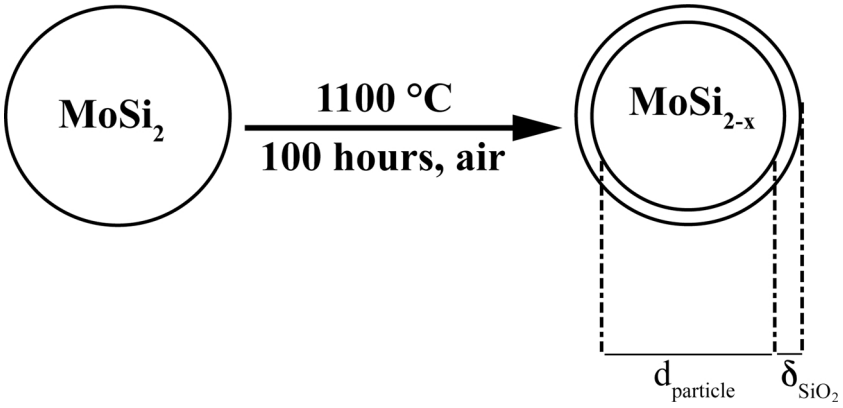

Fig. 9. Schematic of a spherical $MoSi_2$ particle after oxidation test at 1100 °C, 100 h in synthetic air used to calculate the thickness of the formed SiO_2 layer.

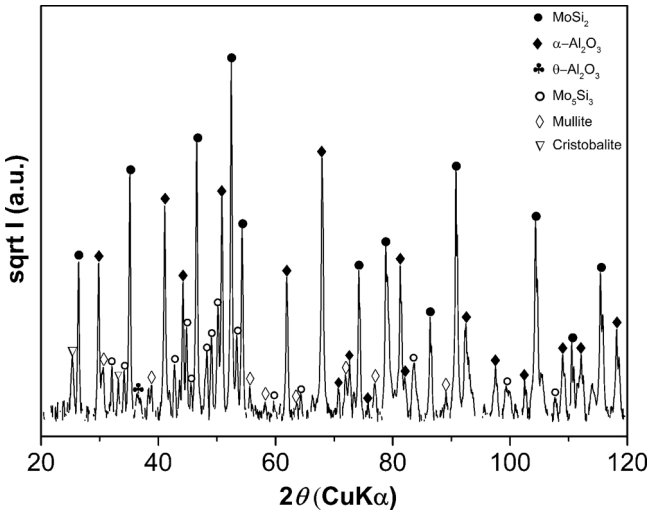

Fig. 10. X-ray diffraction pattern of alumina coated $MoSi_2$ particles calcined at 1200 °C, after shell stability test at 1100 °C, 100 h in synthetic air (20 vol.% O_2 in N_2).

309849, SAMBA. The authors thank Ing. R. W. A. Hendrikx for the XRD analysis.

References

[1] P.R. Taleghani, S.R. Bakhshi, M. Erfanmanesh, G.H. Borhani, R. Vafaei, Improvement of $MoSi_2$ oxidation resistance via boron addition: fabrication of MoB/$MoSi_2$ composite by mechanical alloying and subsequent reactive sintering, Powder Technol. 254 (2014) 241–247.

[2] A.T. Chaharsoughi, G. Borhani, R. Tahmasebi, Structural characterization of $MoSi_2$ synthesized by high-energy mechanical milling followed by annealing heat treatment, J. Alloys Compd. 509 (5) (2011) 2617–2620.

[3] G. Cabouro, S.Le Gallet, S. Chevalier, E. Gaffet, Y. Grin, F. Bernard, Dense MoSi2 produced by reactive flash sintering: control of Mo/Si agglomerates prepared by high-energy ball milling, Powder Technol. 208 (2) (2011) 526–531.

[4] P. Feng, X. Wang, Y. He, Y. Qiang, Effect of high-temperature preoxidation treatment on the low-temperature oxidation behavior of a MoSi2-based composite at 500 °C, J. Alloys Compd. 473 (1–2) (2009) 185–189.

[5] E. Summers, A.J. Thom, B. Cook, M. Akinc, Extrusion and selected engineering properties of Mo–Si–B intermetallics, Intermetallics 8 (9–11) (2000) 1169–1174.

[6] A.K. Vasudevan, J.J. Petrovic, A comparative overview of molybdenum disilicide composites, Mater. Sci. Eng. A 155 (1) (1992) 1–17.

[7] Z. Derelioglu, A.L. Carabat, G.M. Song, S. van der Zwaag, W.G. Sloof, On the use of B-alloyed $MoSi_2$ particles as crack healing agents in yttria stabilized zirconia thermal barrier coatings, J. Eur. Ceram. Soc. 35 (16) (2015) 4507–4511.

[8] F. Nozahic, D. Monceau, C. Estournès, Thermal cycling and reactivity of a $MoSi_2$/ZrO_2 composite designed for self-healing thermal barrier coatings, Mater. Des. 94 (2016) 444–448.

[9] M. Belmonte, Advanced ceramic materials for high temperature applications, Adv. Eng. Mater. 8 (8) (2006) 693–703.

[10] F. Cernuschi, P. Bison, A. Moscatelli, Microstructural characterization of porous thermal barrier coatings by laser flash technique, Acta Mater. 57 (12) (2009) 3460–3471.

[11] N.P. Padture, M. Gell, E.H. Jordan, Thermal barrier coatings for gas-turbine engine applications, Science 296 (5566) (2002) 280–284.

[12] W.G. Sloof, T.J. Nijdam, On the high-temperature oxidation of MCrAlY coatings, Int. J. Mater. Res. 100 (10) (2009) 1318–1330.

[13] T.S. Hille, T.J. Nijdam, A.S.J. Suiker, S. Turteltaub, W.G. Sloof, Damage growth triggered by interface irregularities in thermal barrier coatings, Acta Mater. 57 (9) (2009) 2624–2630.

[14] L.B. Chen, Yttria-stabilized zirconia thermal barrier coatings—a review, Surf. Rev. Lett. 13 (05) (2006) 535–544.

[15] J.D. Osorio, A. Toro, J.P. Hernandez-Ortiz, Thermal barrier coatings for gas turbine aplications: failure mechanism and key microstructural features, DYNA 79 (2012) 149–158.

[16] W.G. Sloof, S.R. Turteltaub, A.L. Carabat, Z. Derelioglu, S.A. Ponnusami, G.M. Song, Crack-healing in yttria stabilized zirconia thermal barrier coatings, Self Healing Materials - Pioneering Research in the Netherlands, IOS Press under the imprint Delft University Press, 2015, pp. 219–227.

[17] S.C. Singhal, Advances in solid oxide fuel cell technology, Solid State Ionics 135 (1–4) (2000) 305–313.

[18] M. Munro, Evaluated material properties for a sintered alpha-alumina, J. Am. Ceram. Soc. 80 (8) (1997) 1919–1928.

[19] A.H. Heuer, Oxygen and aluminum diffusion in α-Al_2O_3: how much do we really understand? J. Eur. Ceram. Soc. 28 (7) (2008) 1495–1507.

[20] Y. Oishi, W.D. Kingery, Self-diffusion of oxygen in single crystal and polycrystalline aluminum oxide, J. Chem. Phys. 33 (2) (1960) 480–486.

[21] A.L. Carabat, S. van der Zwaag, W.G. Sloof, Creating a protective shell for reactive $MoSi_2$ particles in high-temperature ceramics, J. Am. Ceram. Soc. 98 (8) (2015) 2609–2616.

[22] E. Geuzens, G. Vanhoyland, J. D'Haen, S. Mullens, J. Luyten, M.K. van Bael, H. van den Rul, J. Mullens, Synthesis of zirconia–alumina and alumina–zirconia core–shell particles via a heterocoagulation mechanism, J. Eur. Ceram. Soc. 26 (15) (2006) 3133–3138.

[23] W.J. Tang, Z.Y. Fu, J.Y. Zhang, W.M. Wang, H. Wang, Y.C. Wang, Q.J. Zhang, Fabrication and characteristics of TiB_2/Al_2O3 core/shell particles by hybridization, Powder Technol. 167 (3) (2006) 117–123.

[24] M. Jayasankar, S. Ananthakumar, P. Mukundan, W. Wunderlich, K.G.K. Warrier, Al_2O_3 @ TiO_2—a simple sol–gel strategy to the synthesis of low temperature sintered alumina–aluminium titanate composites through a core–shell approach, J. Solid State Chem. 181 (10) (2008) 2748–2754.

[25] F. Dumeignil, K. Sato, M. Imamura, N. Matsubayashi, E. Payen, H. Shimada, Modification of structural and acidic properties of sol–gel-prepared alumina powders by changing the hydrolysis ratio, Appl. Catal. A 241 (1–2) (2003) 319–329.

[26] H. Kim, M. Chen, Q. Yang, T. Troczynski, Sol–gel alumina environmental barrier coatings for SiC grit, Mater. Sci. Eng. A 420 (1–2) (2006) 150–154.

[27] Q. Yang, T. Troczynski, Dispersion of alumina and silicon carbide powders in alumina sol, J. Am. Ceram. Soc. 82 (7) (1999) 1928–1930.

[28] B.E. Yoldas, Alumina gels that form porous transparent Al_2O_3, J. Mater. Sci. 10 (11) (1975) 1856–1860.

[29] C.-Y. Yang, W.-H. Shih, Effect of acid on the coating of Boehmite onto silicon carbide particles in aqueous suspensions, J. Am. Ceram. Soc. 82 (2) (1999) 436–440.

[30] Y.T. Zhu, M. Stan, S.D. Conzone, D.P. Butt, Thermal oxidation kinetics of $MoSi_2$-based powders, J. Am. Ceram. Soc. 82 (10) (1999) 2785–2790.

[31] A.A. Sharif, High-temperature oxidation of $MoSi_2$, J. Mater. Sci. 45 (4) (2010) 865–870.

[32] J.A. Wang, X. Bokhimi, A. Morales, O. Novaro, T. López, R. Gómez, Aluminum local environment and defects in the crystalline structure of sol − gel alumina catalyst, J. Phys. Chem. B 103 (2) (1999) 299–303.

[33] A.P. Ferreira, D. Zanchet, R. Rinaldi, U. Schuchardt, S. Damyanova, J.M.C. Bueno, Effect of the CeO_2 content on the surface and structural properties of CeO_2–Al_2O_3 mixed oxides prepared by sol–gel method, Appl. Catal. A 388 (1–2) (2010) 45–56.

[34] A.F. Popa, S. Rossignol, C. Kappenstein, Ordered structure and preferred orientation of boehmite films prepared by the sol–gel method, J. Non-Cryst. Solids 306 (2) (2002) 169–174.

[35] I. Levin, D. Brandon, Metastable alumina polymorphs: crystal structures and transition sequences, J. Am. Ceram. Soc. 81 (8) (1998) 1995–2012.

[36] J.G. Li, X. Sun, Synthesis and sintering behavior of a nanocrystalline α-alumina powder, Acta Mater. 48 (12) (2000) 3103–3112.

[37] B.C. Lippens, J.H. De Boer, Study of phase transformations during calcination of aluminum hydroxides by selected area electron diffraction, Acta Crystallogr. 17 (10) (1964) 1312–1321.

[38] Q. Yang, T. Troczynski, Alumina sol-assisted sintering of SiC—Al_2O_3 composites, J. Am. Ceram. Soc. 83 (4) (2000) 958–960.

[39] P. Fielitz, G. Borchardt, M. Schmücker, H. Schneider, P. Willich, Measurement of oxygen grain boundary diffusion in mullite ceramics by SIMS depth profiling, Appl. Surf. Sci. 203 (2003) 639–643.

[40] S. Chevalier, B. Lesage, C. Legros, G. Borchardt, G. Strehl, M. Kilo, Oxygen diffusion in alumina. Application to synthetic and thermally grown Al_2O_3, Defect Diffus. Forum 237–240 (2005) 899–910.